frontiers | Frontiers in Earth Science

TYPE Original Research
PUBLISHED 25 August 2022
DOI 10.3389/feart.2022.881138

OPEN ACCESS

EDITED BY
Lara S Wagner,
Carnegie Institution for Science (CIS),
United States

REVIEWED BY
Thomas Merry,
Imperial College London,
United Kingdom
Colton Lynner,
University of Delaware, United States

*CORRESPONDENCE
S. Salimbeni,
simone.salimbeni@ingv.it

SPECIALTY SECTION
This article was submitted to Solid Earth Geophysics,
a section of the journal
Frontiers in Earth Science

RECEIVED 22 February 2022
ACCEPTED 05 July 2022
PUBLISHED 25 August 2022

CITATION
Salimbeni S, Pondrelli S, Molinari I, Stipčević J, Prevolnik S and Dasović I (2022), Seismic anisotropy across Adria plate, from the Apennines to the Dinarides.
Front. Earth Sci. 10:881138.
doi: 10.3389/feart.2022.881138

Seismic anisotropy across Adria plate, from the Apennines to the Dinarides

S. Salimbeni[1]*, S. Pondrelli[1], I. Molinari[1], J. Stipčević[2], S. Prevolnik[2], I. Dasović[2] and the AlpArray-CASE working group

[1]Istituto Nazionale di Geofisica e Vulcanologia, Sez, Bologna, Italy, [2]Department of Geophysics, Faculty of Science, University of Zagreb, Zagreb, Croatia

The Adria microplate has the particular feature to be involved in two subduction systems with slab dipping in opposite directions, one toward west beneath the Apennines and the other to the east beneath the Dinarides. The deep structure of Adria and the shape and characteristics of the slabs have mainly been studied through seismic tomography. However, the uncertainty about the presence and dimensions of tear and windows along the Apennines and the Dinarides slabs is still large. An instrument that can be used to draw mantle flows and to support the possible presence of slab windows or tears is the detection of seismic anisotropy, in particular core phases shear wave splitting. In this paper, to give more light to the structure of Adria slabs and possible mantle circulation beneath this microplate, we benefit from data recorded by seismic stations located along a profile running across the central Adriatic from the Apennines to the edge of the Panonnian basin. The new measurements, together with previous findings, show an evident change of the anisotropic properties when moving along the profile. The distribution of SKS-splitting measurements in the Apennines strongly agree with previous measurements that already described the toroidal flow generated by the slab rollback of the Calabrian arc. In addition, the N-S and NE-SW directions found beneath the Apulia are in agreement with those attributed previously in the outer northern Apennines, to a proper typical pattern of the mantle beneath Adria, which is undeformed by the slab retreat. The pattern of the anisotropy in the Dinarides region shows lateral and vertical variations that together with recent tomographic images that better define the slab window allow us to speculate as follows: the new SKS measurements, interpreted in terms of mantle deformation and flows, agree with the geodynamic model that justifies the mantle circulation beneath Adria with the presence of slab windows in both the Apennines and Dinarides slabs.

KEYWORDS

seismic anisotropy, subduction, lithosphere, asthenosphere, Adria plate, AlpArray

Introduction

The Western/Central Mediterranean area is a complex subduction zone where the African and Eurasian plates interact. This interaction is complicated by the presence of the Adria plate (Figure 1A) that lies in-between and which is the continental lithosphere foreland shared by the Africa-Eurasia convergence zone in the north (Alps) and by two subduction zones (Apennines and Dinarides) with slabs that dip in opposite directions. The subduction in the Dinarides was active from the early Cretaceous to the Paleogene, and it was followed by lithospheric delamination in the north and central part of the chain from the late Eocene (Handy et al., 2015, 2019). The subduction is only still active in its southern part (i.e., Hellenides), as confirmed by the tomography and the presence of deep earthquakes (Handy et al., 2015). The subduction in the Apennines started later (from the late Eocene to the present) with process dominated by the slab rollback as a consequence of the subduction of the Ionian oceanic crust starting from the 8–10 Ma (Goes et al., 2004; Faccenna, 2005). It is considered to be still active beneath the northern Apennines and the Calabrian arc (Faccenna and Becker, 2020).

The Adria plate is therefore the lower plate in the interaction with the Apennines and the Dinarides, while it is the upper plate in the interaction with the western and central Alps (Figure 1B). Currently, it moves toward north/northwest with a counter-clockwise rotation around an Eulerian pole that is located in the western Alps at a rate of 0.25°/My for Serpelloni et al. (2005) or in Spain for Le Breton et al. (2017). Tomographic images show

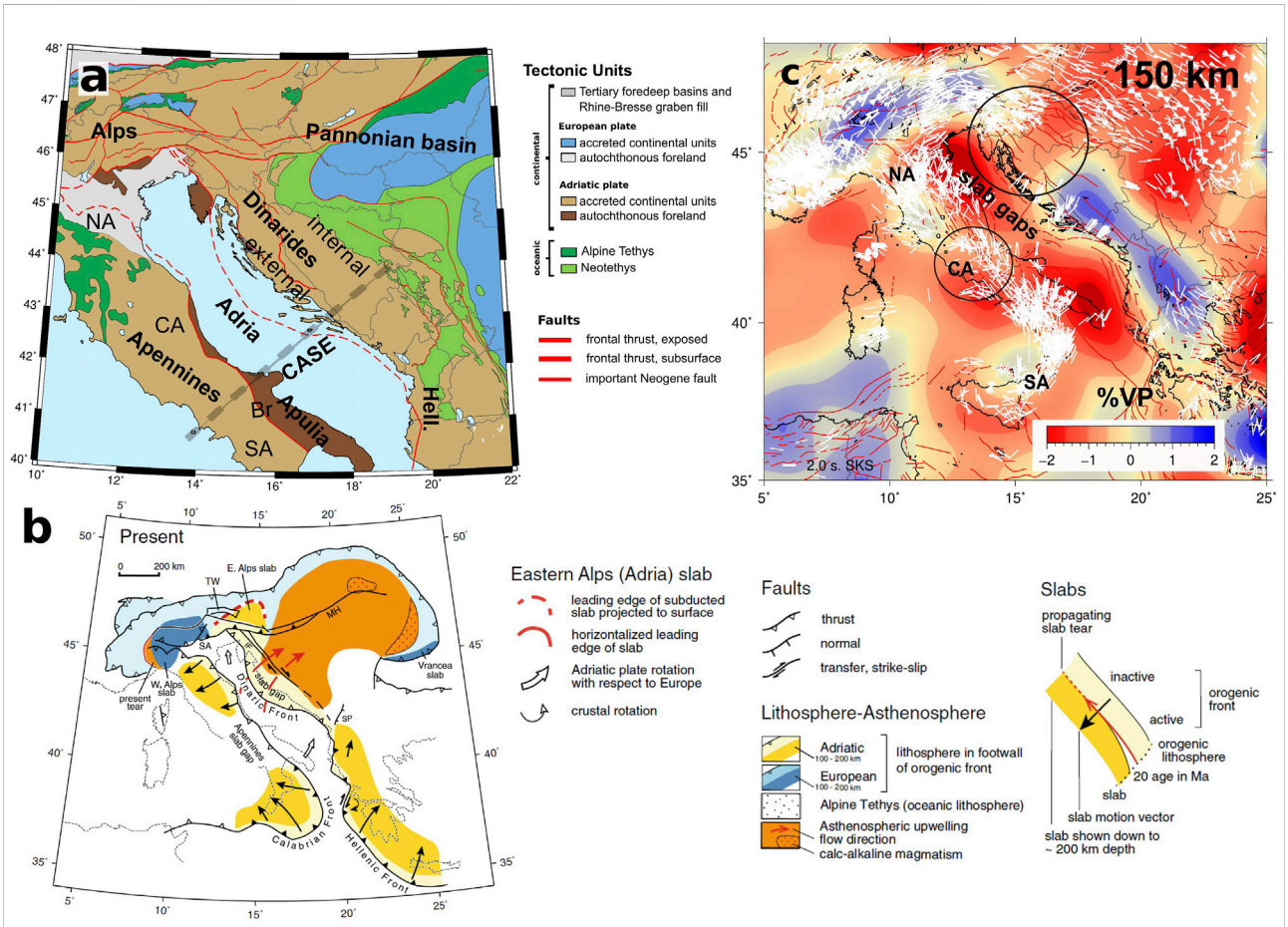

FIGURE 1
(A) Maps of the tectonic unit of the Alps-Apennines-Dinarides-Hellenic area freely modified from the original compilation of M.R. Handy with units and major lineaments simplified from Schmid et al. (2004, 2008), Handy et al. (2010, 2015, 2019), Bigi et al. (1990), Froitzheim et al. (1996), and Bousquet et al. (2012). NA, CA, SA = northern, central, and southern Apennines; Br = Brandanic foredeep. **(B)** Slab maps for the Alpine chain with upper plates removed and only major faults shown. Northward subduction of Adriatic lithosphere beneath Eastern Alps and shortening of the Pannonian basin (modified from Handy et al., 2015). **(C)** Tomographic sections at 150 km of depth of the circum-Adriatic region as imaged by Piromallo and Morelli (2003) with the superimposition of the shear wave splitting measurements of the area taken from SplitLab database (Barruol et al., 2009; Wüstefeld et al., 2009) in the years before the CASE project started. Each white line corresponds to one single measurement oriented parallel to the fast axes and scaled with the delay time and plotted at the same tomographic layer depth.

this complexity and document the presence of slabs beneath the Dinarides and the Apennines (Bijwaar and Spakman, 2000; Piromallo and Morelli, 2003; El-Sharkawy et al., 2020). Beneath the Italian peninsula, most tomography images agree about the presence of two high velocity bodies (Figure 1C), which are interpreted as slabs, beneath the northern Apennines and Calabrian arc, continuous from top to the bottom of the upper mantle and which are the results of the subduction of the Adriatic and Ionian lithospheres beneath the Apennines and Calabrian arc, respectively (El-Sharkawy et al., 2020, and references therein). In the central Apennines a low velocity region is present at shallow depth (from 70 to 200 km), which is interpreted as a possible slab window due to a tear of the Calabrian arc slab in its shallow NW part (Faccenna et al., 2014). However, deeper (from 250 km downward) tomographic images show that Northern Apennines and the Calabrian arc slabs are linked in a unique high velocity body (El-Sharkawy et al., 2020). In the Dinarides region, most of the tomographic images of the eastern Adriatic coastal zone agree with the presence of a continuous high velocity body in shallower part, down to 150 km (Piromallo and Morelli, 2003; Li et al. 2008) that extends all along the Dinaric chain and which reaches depth of 300 km in correspondence to the Albanides/Hellenides region (Figure 1C). Beneath the northern and central Dinarides, between 150 and 300 km depth, a low velocity zone is present, which supports the idea of the existence of a slab gap. The location and dimension of this velocity anomaly differ between tomographies, in some cases it is shown as wider (Bijwaard and Spakman, 2000; El-Sharkawy et al. 2020), and in other cases it is shown as narrower (Piromallo and Morelli, 2003).

The presence and dimensions of tears or slab windows are supported by mantle deformation studies, which are usually based on SKS shear wave splitting measurements. It is well-known that mantle rocks are mostly composed of anisotropic minerals, mainly olivine, that tend to align with the deformation field (Mainprice et al., 1993). Core refracted phases, such as SKS from teleseismic events, are sensitive to the orientation of olivine crystals and, when crossing the anisotropic material, it splits into two phases that travel with different velocity. The polarization direction of the faster phase and the time delay between the arrivals of the two phases are the parameters that are used to define the seismic anisotropy properties in a region beneath a seismic station (Savage, 1999). SKS analysis on a great number of stations yields anisotropy patterns related to the upper-mantle deformation, which in a subduction system are correlated with mantle flows (i.e., toroidal flows through slab discontinuities or around slab edges) (Civello and Margheriti, 2004; Long and Becker, 2010; Porritt et al., 2014; Schlaphorst et al., 2017). Indeed, under most upper-mantle conditions, we expect A-type olivine LPO, which means that the fast direction is aligned with mantle flow directions or shear planes (Long and Becker, 2010).

Shear wave splitting measurements in the region of interest are already available, mainly for the Italian peninsula, with few results in the Dinaric region (Figure 1C). Seismic anisotropy patterns depict the complexity of the mantle deformation beneath the Apennines. The southern (SA) and the northern Apennines (NA) are active subduction zones that have different characteristics. In the south, the subduction is defined to be still active because of the presence of deep seismicity (down to 500 km, Chiarabba et al., 2005), active volcanism (Aeolian arc), and high rate of convergence (10 mm/y, Serpelloni et al., 2005). The distribution of the splitting parameters is described in several studies (Margheriti 1998; Margheriti et al., 2003; Civello and Margheriti, 2004; Baccheschi et al., 2007, 2008, 2011) and it is interpreted as the effect of the E-SE retreat of the Calabrian arc, which generates trench-parallel fast axes direction in the sub-slab mantle and trench-perpendicular direction in the back-arc region. Similar patterns are observed in other subduction systems (Savage, 1999) and in laboratory experiments (Buttles and Olson, 1998; Funiciello et al., 2006).

The northern Apennines (NA) exhibits different characteristics. The volcanism in this region is old or absent, the convergence rate is slower (1 mm/y, Serpelloni et al., 2005), and most of the seismicity is located in the first 15 km depth (Chiarabba et al., 2005). Deeper seismicity was observed but shallower than 90 km (Selvaggi and Amato, 1992). The distribution of the splitting parameters in this region is very complex (Margheriti et al., 2003; Plomerová et al., 2006, Salimbeni et al., 2007, 2008, 2013), with trench-parallel directions found in the back-arc zone and trench-perpendicular in the opposite side. In particular, the scattering in the fast axes directions and the variability of the delay times in the Po-Plain area evidence the presence of a complex upper-mantle structure that is generated by the interaction between the Apennines, the Alps, and the Dinarides (Qorbani et al., 2015, 2016; Song et al., 2019; Petrescu et al. 2020a, 2020b). Salimbeni et al. (2008) hypothesized that this pattern is related to an oblique trench-retreat of the northern Apennines slab toward the east, due to the lack of space because of the presence of the Alpine subduction system to the north and the subduction beneath the Dinaric belt behind. Thus, the pattern of seismic anisotropy in the northern Apennines is different from that in the southern part of the chain (Salimbeni et al., 2013).

In the central Apennines and in the Dinaric region, the available seismic anisotropy dataset is quite poor, and consequently inferences about the upper-mantle deformations comes from sparse results (Margheriti, 1998; Margheriti et al. 2003; Subašić et al., 2017). The complementary "Central Adriatic Seismic Experiment" (CASE; Molinari et al., 2018), which was developed within the framework of the AlpArray project (Hetényi et al., 2018), gave an opportunity to extend the shear wave splitting dataset for this region. CASE consisted of 10 temporary stations installed in Bosnia and Herzegovina, Croatia, and Italy for 2 years.

In this paper, we use the shear wave splitting measurements (on SKS phases) obtained from CASE and other permanent

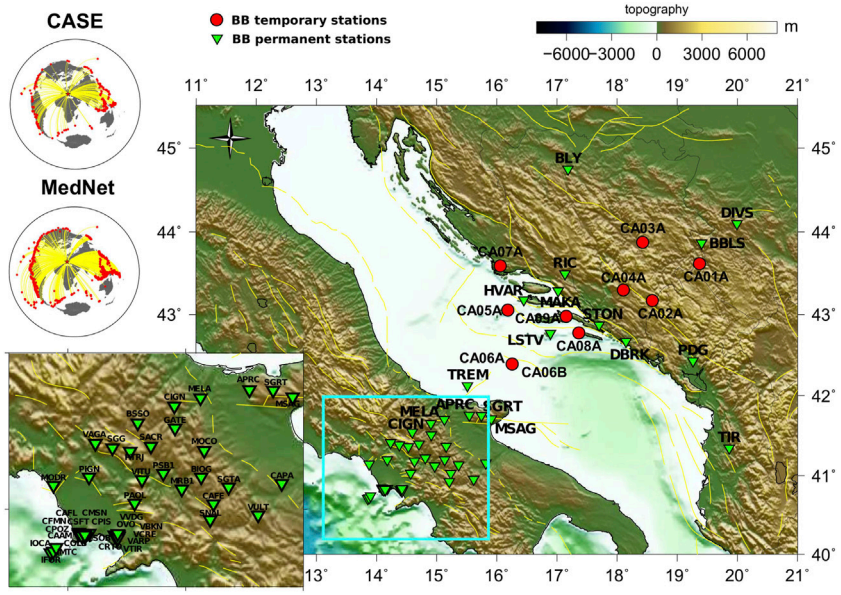

FIGURE 2
Map of the AlpArray-CASE broadband seismic stations used in this work. The permanent stations, belonging to MedNet and Italian, Croatian, and Republic of Srpska national seismic networks, are represented by green triangles; the temporary stations deployed for the AlpArray-CASE are represented with red circles. (Upper inset) The back-azimuthal distribution of the teleseismic events for the MedNet and the other networks used in the analysis.

stations data to increase the definition of seismic anisotropy patterns in the Central Adriatic region and refine our knowledge of slab extension and discontinuities and of the related mantle flows.

Data and methods

Records from 237 teleseismic events that occurred between November 2016 and December 2018, with M > 5.8 within epicentral distance range of 85°–120°, are recovered from the temporary stations of the AlpArray-CASE project (red circles in Figure 2) and permanent stations belonging to the Italian and the Croatian national seismic network (green triangles in Figure 2). The back-azimuthal distribution of the events is summarized in the inset of Figure 2. Taking advantage of the long lasting MedNet seismic stations (Pondrelli et al., 2020), four of which are located in the region of interest (TIR, BLY, PDG, and DIVS), we collected and analyzed a large number of earthquake recordings, 1,037 events with M ≥ 6 occurred between October 2004 and November 2016.

The shear wave splitting analysis was performed with the SplitRacer software (Reiss and Rümpker, 2017), which is a MATLAB graphical user interface environment that is designed to analyze large amounts of teleseismic data. The code automatically performs an initial preprocessing in which the quality of the data is inspected (i.e., check for gaps, correctness of the travel time of the interested phases, value of signal-to-noise ratio) and then visually selected to choose the correct time window. In our analysis, at this point, all of the data have been filtered using the same bandpass frequency window, which is useful to enhance the amplitude of the S-wave (with corner frequency 7–20 s). The last step of preprocessing is the correction of waveforms for possible misalignment of the horizontal components, comparing the particle motion of the phase with the theoretical back-azimuth of the event taken into account. All suitable data are then analyzed, and the fast axes and delay time parameters are determined using the energy minimization on the transverse component (Silver and Chan, 1991), each time applied over 50 slightly shifted time windows, as suggested by the developer. Silver and Chan's (1991) technique is considered to be the most robust for core refracted teleseismic phases, such as SKS, in which the back-azimuth is readily known.

To obtain a robust and realistic database of the splitting parameters, all of the results were visually inspected. The splitting measurement is considered valid 1) if the phase selected is well isolated, 2) the signal-to-noise ratio (SNR) is greater than 3, 3) if the energy on the transverse component is present, 4) if the ellipticity of the particle motion is sufficiently linearized after the removal of the delay time, and 5) if original and corrected waveforms are in agreement. Each measurement is then selected if it has a reasonable distribution of errors. In addition, we consider results acceptable when the delay time is lower than 3 s. Along with these criteria, the result is defined as

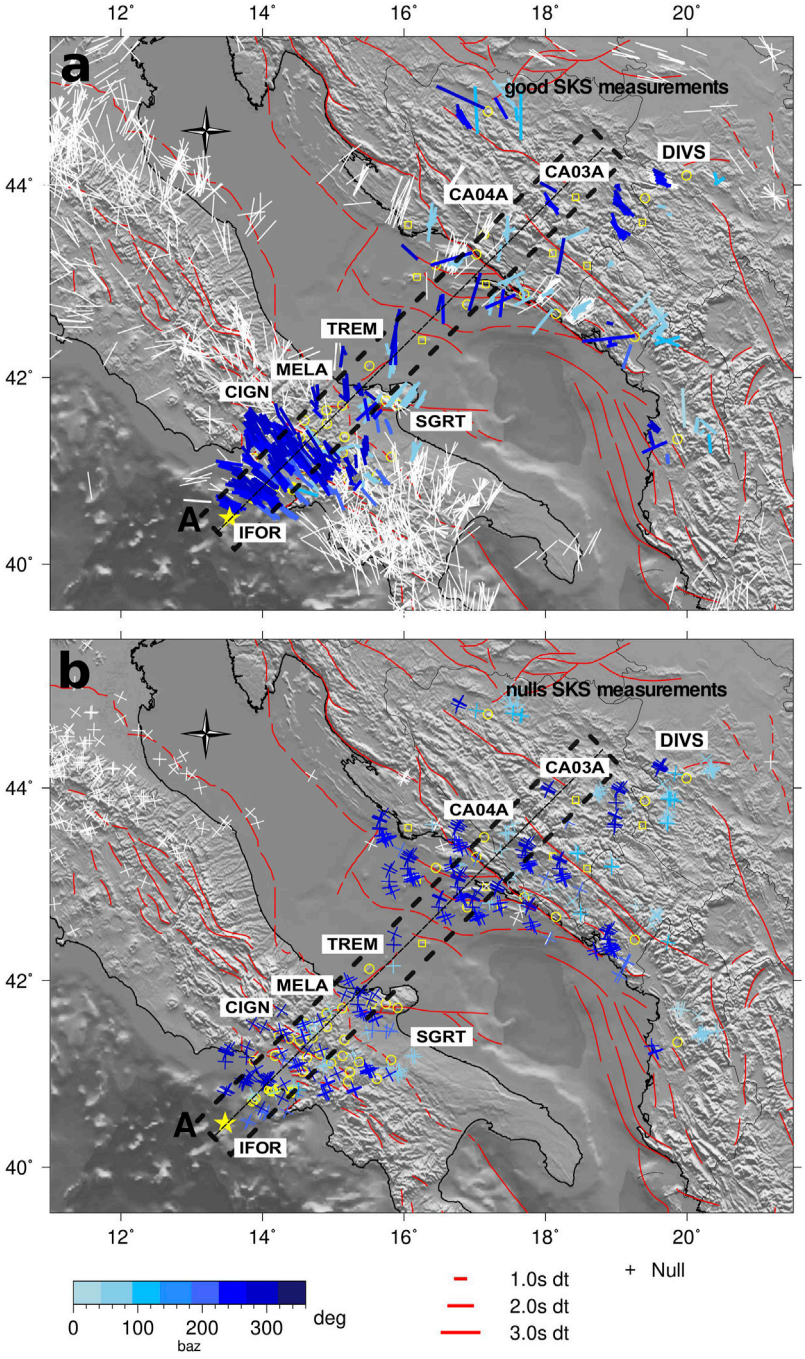

FIGURE 3
Map of the obtained results. **(A)** Single shear wave splitting measurements of "good" quality are plotted as line oriented parallel to the fast axes and scaled with the delay time value. **(B)** Null measurements obtained and plotted as crosses with branches parallel and perpendicular to the back-azimuth of the analyzed event. In both maps, yellow circles and squares are temporary and permanent stations composing the network used, results of the CASE project are plotted following the back-azimuth color scale while results from previous works are plotted in white (from SplitLab database; Barruol et al., 2009; Wüstefeld et al., 2009). Trace of the section (with its 40-km swath box) used for the following interpretation is mapped with the dashed line. Starting point of the trace is represented by the yellow star and labeled with the "A", the station name used in the map is referred to those stations limiting the anisotropic boundaries.

"good" when the energy reduction is greater than 80%, "average" when the energy reduction is 60 to 80%, and "poor" in all other cases. In the absence of energy on the transverse component or in case of its presence when splitting was precluded (e.g., when the fast axis is oriented perpendicular or parallel to the back-azimuth of the analyzed earthquake), the result is classified as a "null" measurement. An example of a "good" quality shear wave splitting and a "null" measurement are shown in Supplementary Figure S1A,B, respectively.

Results

Single and mean shear wave splitting distribution

The results of the shear wave splitting analysis performed on the entire dataset are summarized in Supplementary Figure S2 and listed in Supplementary Table S1, S2. However, to guarantee the best reliable image of seismic anisotropy of the study region, we will focus only on measurements that we defined as "good" and on "null" data given by SKS phases that showed the best quality. The distribution of these results is mapped in Figure 3.

In Figure 3A, the new 585 single shear wave splitting measurements of "good" quality are plotted as single line oriented parallel to the fast axes and scaled with the delay time value. The color scale used to plot the measurements is in agreement with the back-azimuth of the analyzed events. Measurements in white are taken from previous works and collected in the SplitLab database (Barruol et al., 2009; Wüstefeld et al., 2009). In Figure 3B, the 448 null measurements are plotted as crosses with their lines oriented parallel and perpendicular to the back-azimuth of the analyzed event. In both maps, all measurements are projected into the upper-mantle depth (150 km).

The distribution of the single shear wave and null measurements agree with the distribution of fast axes and delay time obtained in previous works, where available. In the Tyrrhenian coast and in the internal part of the Apennines, the fast axes show a homogeneous rotation from E-W to NW-SE direction. These orientations are similar to those found all along the internal region of the whole chain, both in the north (Margheriti et al., 2003; Salimbeni et al. 2008, *and references therein*) and in the south (Baccheschi et al. 2011), and parallel to the E-W stretching direction related to the back-arc basin extension (Lucente et al., 2006). Moving toward the Adriatic coast, the fast axis direction rotates clockwise toward N and NE upon entering the Dinarides region, which confirms the results published by Margheriti et al. (2003) and Subašić et al. (2017). Moving towards the internal part of the Dinarides, the direction of fast axes rotates back to NW-SE, parallel to the strike of the chain and to the strike of the major faults located in the area. This direction agrees well with the results obtained by Qorbani et al. (2016), Song et al. (2019), and Petrescu et al. (2020b) for the Carpathian-Pannonian region and, extending toward east, with those by Ivan et al. (2008) in the Romanian region. The distribution of the null measurements corroborates this fast axis distribution, as shown in Figure 3B.

For each station with more than two good splitting measurements, we calculate the average value for fast axes and delay time. The average delay time is calculated with the standard arithmetic mean and the results are shown in Figure 4A (and listed in Supplementary Table S3). Stations with higher values of dt (shown in light green and in red) are concentrated only beneath the Apennines chain while values lower than 1.5 s (in dark green and blue) are mainly obtained beneath Apulia, Adriatic, and the Dinarides areas. The error associated with the average dt varies from 0.04 s (VCRE station) to 0.86 s (STON station). The mean fast axes direction is instead calculated using the circular statistics as the mean direction of the vector resulting from a group of directional data (Davis, 2002) and with the error attributed as its mean resultant length (R), which represents the spreading of the vectors around its mean value (R = 0, distribution completely scattered around the mean value, R = 1 distribution completely aligned with the mean value; Figure 4B and Supplementary Table S3). The rotation of the fast axes detected in the distribution of single measurements is even more evident when looking at the mean directions. In the inner part of the Apennines and in the internal part of the Dinarides (i.e., the extremes of the transect), the mean fast axes direction is NW-SE with a distribution that is tightly bunched around the mean value (R>=0.8, shown in red in Figure 4B). In between, the main direction rotates clockwise toward N-S and NNE-SSW with lower values of R, meaning a more scattered single measurements distribution around its mean fast axis direction (green and blue sticks in Figure 4B).

Shear wave splitting parameters along the CASE transect

To define the position where changes in anisotropic direction occur, we focus on the distribution of the shear wave splitting parameters along the CASE profile (dashed line in Figure 3 and in Figure 1A). All the splitting parameters included in the 40-km-wide box (dashed-line box in Figure 3) are projected along the transect and are plotted as a function of the distance from the starting point (star with A label in Figure 3). The section is shown in Figure 5 where, from top to bottom, topographic profile (A), fast axes (B), and delay time (C) distributions are shown.

Looking at the results shown in Figure 5, starting from SW (Apennines) and based on the homogeneity of the distribution of the splitting measurements, it is possible to define four anisotropic homogeneous domains.

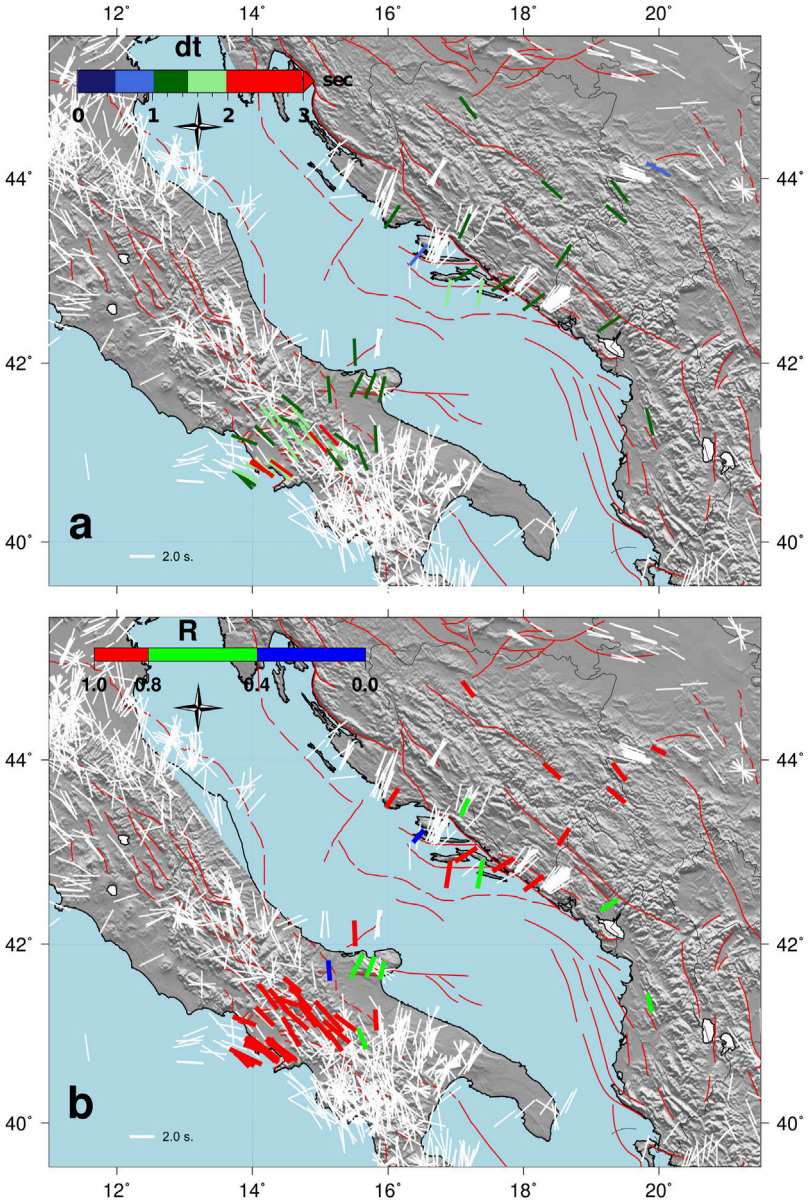

FIGURE 4
Distribution of shear wave splitting measurements averaged with arithmetic and circular statistics for each station of the CASE project with at least two good measurements. Results for each station are represented with scale color for **(A)** delay time and **(B)** R value (i.e., the spread of the vectors around its mean value). The results from previous works taken from SplitLab database are given in white (Barruol et al., 2009; Wüstefeld et al., 2009).

Domain 1 (from IFOR to CIGN stations): the fast axes are mainly oriented in NW-SE direction (with some N-S or E-W scattered direction), while the delay time varies from 0.5 to almost 3 s. The average fast axis direction (red squares) varies from −70° to −40° (with R from 0.65 to 1) between single stations, the mean delay time is in the range 1–2.5 s (with errors from 0.04 to 0.62 s). These SKS-splitting directions do not show any particular dependence (e.g., from the back-azimuth) even if most of the null measurements are obtained for events coming from 60° and −80° directions.

Domain 2 (from MELA to SGRT stations): the single fast axis direction varies from WNW to ENE (−60° to 60°), while the delay time for single measurement is between 0.5 and 2.5 s. The average fast axes vary from 0° to 20° (with R between 0.39 and 0.81) and the mean dt is 1–1.5 s (with errors between 0.19 and 0.5 s), which are both representative of a sparser single shear wave splitting

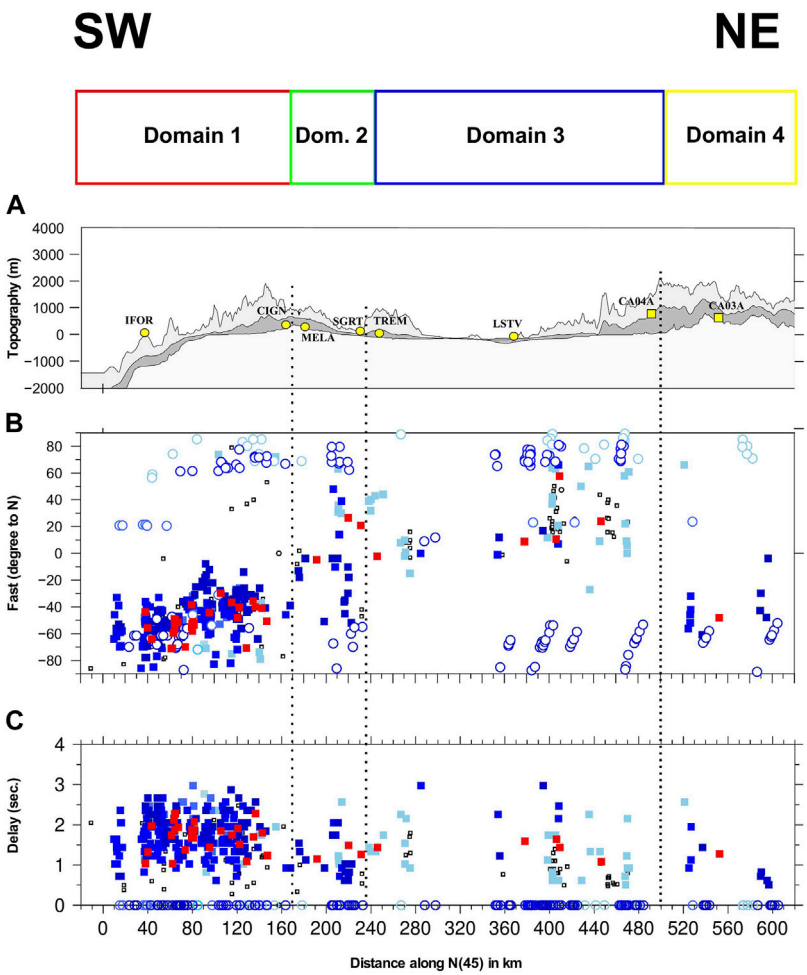

FIGURE 5
Distribution of fast axes and delay time along the CASE profile mapped in Figure 3. From top to bottom, panels representing the boundaries of the anisotropic domains, the topographic profile with the station name **(A)**, the distribution of fast axes **(B),** and delay time **(C)** along the profile. In **(B)** and **(C)**, blue squares represent single measurements, red squares are the mean values, and white squares are the results from previous works. Null measurements are plotted as circles using in **(B)** the back-azimuth of the events (instead of the fast axes) and in **(C)** the delay time equal to 0. In **(B)** and **(C)**, single shear wave splittings and null measurements are colored in agreement with the back-azimuth scale from Figure 3.

distribution. Teleseismic events coming from -70° or 70° (±10°) generate most of the null measurements.

Domain 3 (from TREM to CA04A stations): the fast axes distribution is homogeneous with values that vary from N to NE (from 0° to 40°) and the delay times vary from 0.5 to 3 s. The mean fast axis direction varies from 0° to 40° (with R varying between 0.34 and 1) and the mean dt varies from 1 to 3 s (with error between 0.45 and 0.86 s). It is worth noting that here the NW-SE direction disappears completely (direction prevailing in Domain 1 and still present in Domain 2), leaving the place to mostly N-S to NNE-SSW directions. The prevailing back-azimuth direction for the null measurements remains the same as in previous domains.

Domain 4 (from CA03A to DIVS stations): here the most representative fast axis direction is again NW-SE, with a tight orientation distribution from −20° to −40° (and R in the range 0.74–0.95). The same for the delay times, distributed symmetrically around the mean value, ~1 s (i.e., between 0.89 and 1.28 s with errors in the range 0.14–0.49 s). Null measurements are obtained from events with back-azimuths along an E-W direction.

Another point raised by Figure 5 is that most of the SKS-splitting measurements are obtained from a certain back-azimuthal direction. Excluding Domain 1, where the NW-SE direction of fast axes is sampled for each back-azimuthal sector, in all other domains the NE-SW (or ~ N-S) fast axis directions are obtained only from eastern coming teleseisms, while those from other directions sample different fast axis orientations. A confirmation of this trend is found by plotting the rose and polar diagrams of each domain, as shown in

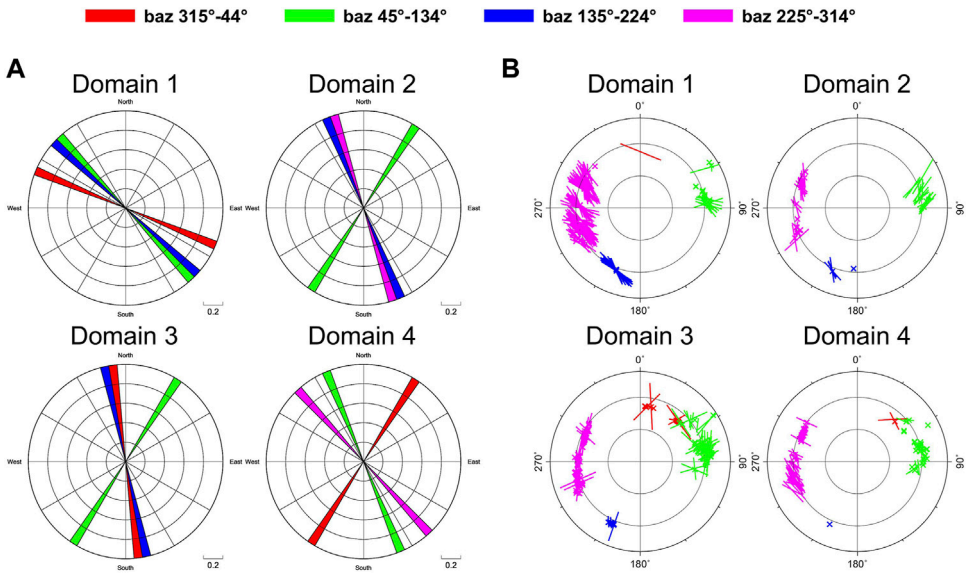

FIGURE 6
(A) Rose diagrams representing the mean fast axes direction calculated for each anisotropic domain and divided by back-azimuth of the events. **(B)** Polar distribution of the fast axes and null measurement for each anisotropic domain. Each result is plotted as lines oriented parallel to the fast axes and located in function of back-azimuth and epicentral distance of the event analyzed.

Figure 6. In the rose diagrams (Figure 6A), shear wave splittings are represented by the mean value calculated over all measurements for each back-azimuthal quarter. In contrast, in the polar plots (Figure 6B) single measurements are plotted with respect to the back-azimuth and epicentral distance. In both types of representation, it is evident that a back-azimuthal dependence is present in all domains, excluding Domain 1 (as previously mentioned). Data of Domains 2, 3, and 4 sample an anisotropy with NE-SW direction only with events coming from N (in red) or NE (in green), while events coming from western back-azimuths sample anisotropy oriented N-S or NNW-SSE. For Domain 4, it is worth noting that most of the teleseisms coming from the western (pink) sector give "good" results; for events coming from the eastern sector (in green), the results are in general of lower quality (and are therefore not included in the polar diagram of Figure 6B) or are null measurements (represented by the green crosses). Based on the back-azimuthal dependence of the measurements (Savage, 1999), we hypothesize the presence of a complex anisotropic structure beneath the stations in the Domain 2, 3, and 4. The recognition of any other specific trend, such as the presence of periodicities in the fast direction and delay time with respect to back-azimuth, that would point to multilayer or dipping structure of the anisotropy is very difficult due to the intermittent back-azimuthal coverage provided by the 2-years of data from the temporary CASE stations.

Discussion

Depth distribution of the anisotropy and comparison with other seismological observables

Anisotropy measurements obtained by SKS-splitting analysis are generally difficult to locate at depth, along the ray path, and they are considered the integral of all of the anisotropy that the seismic waves detect from the core to the surface. However, the study region is located in an active geodynamic framework, with multiple subduction systems evolving at the same time in a quite reduced space. Given that the upper mantle is the place where most of the anisotropy is concentrated (Savage, 1999), we can assume that detected anisotropy is mainly located there, where most changes occur, such as slab discontinuities and mantle flows. An estimation in each domain of the thickness of the anisotropic material crossed by seismic rays may provide additional information. It could be performed using the following formula (Silver and Chan, 1988; Helffrich 1995):

$$L = dt * \beta / k \quad (1)$$

where dt is the delay time (in seconds), β is the shear wave velocity (4.48 km/s for the upper mantle, Kennett et al. 1995), and κ is the anisotropy percentage that in the upper mantle could vary from 4 to 5% (Savage, 1999). Considering that the contribution of the anisotropy in the crust and in the deeper

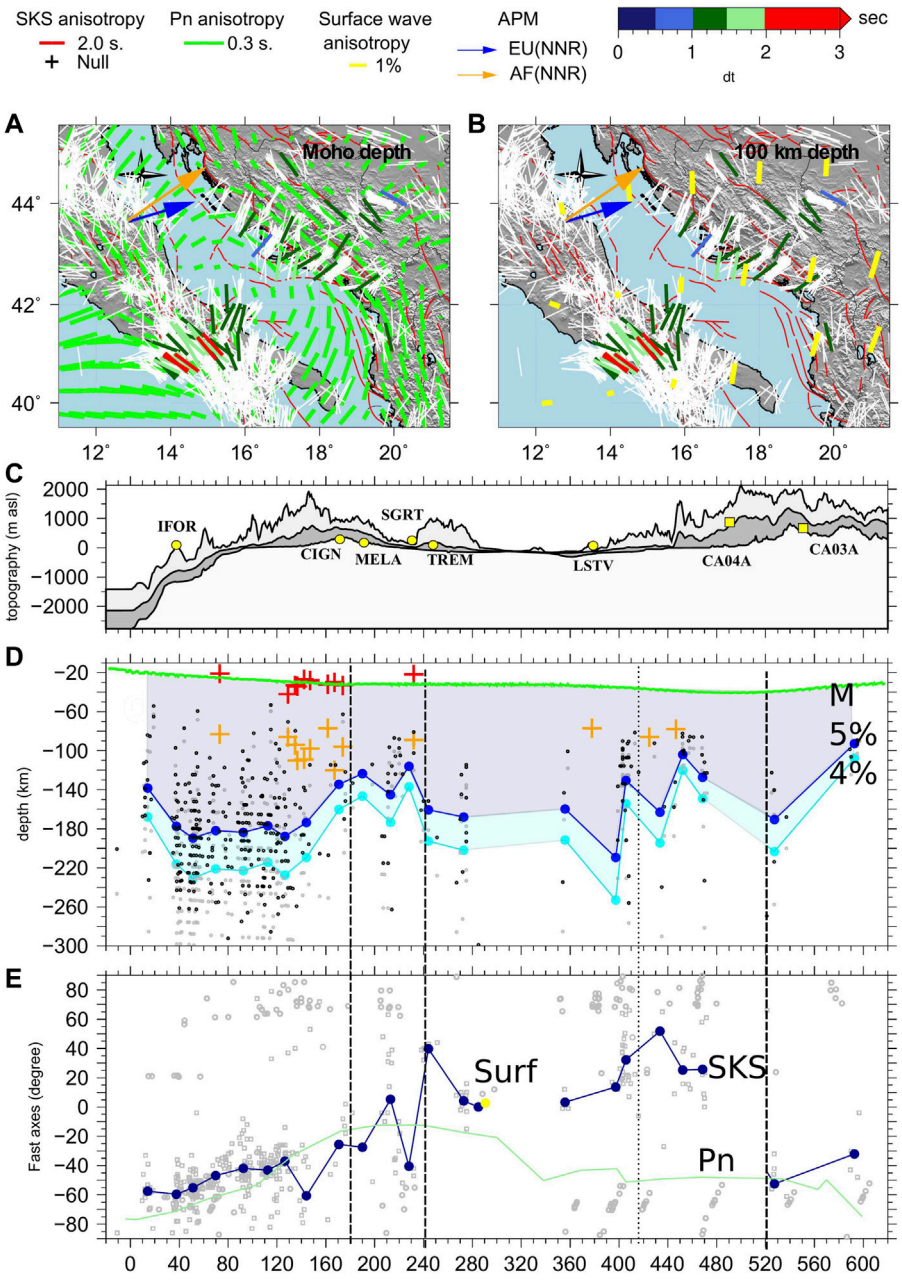

FIGURE 7
(Upper maps) Comparison between averaged SKS measurements (from this and previous works), Pn anisotropy **(A)** (Diaz et al., 2013) and surface wave anisotropy **(B)** (Zhu et al., 2015). The previous splitting parameters taken from the SplitLab database are plotted in white (Barruol et al., 2009; Wüstefeld et al., 2009). Each measurement is oriented parallel to the fast axis while the length of each bar corresponds to delay time (for the Pn) or strength of anisotropy (for surface wave). Delay time for SKS measurements follows the color scheme in the legend. Arrows indicate the Absolute Plate Motion direction of the Eurasian (in blue) and African (in orange) plates in the HS2-NUVEL1A hot-spot reference frame (Gripp and Gordon, 1990; DeMets et al., 1994). (Lower panels) **(C)** The topography of the CASE profile with the name of the stations limiting the domains, and **(D)** location along the CASE profile of the anisotropic layer calculated with formulation (1) and for 5% (light blue volume) and 4% (cyan volume) of anisotropy. Single estimations of the anisotropic volume for the same percentage of anisotropy range are also plotted with dark and gray circles, respectively. In the same plot also the Moho depth (line in green and with "M" label from Molinari et al. (2015) and single red crosses from Miller and Piana Agostinetti (2012)) and the litho-asthenospheric boundary (orange crosses from Miller and Piana Agostinetti (2012) and Belinić et al. (2018)) are plotted. The vertical dashed lines correspond to the boundaries of the anisotropic domains as defined previously. **(E)** Comparison of mean values of SKS (in blue), Pn (in green), and surface wave (single dot in yellow) anisotropies directions all calculated with steps of 20 km along the CASE profile.

part of the mantle is negligible (less than 0.3 s and less than 0.7 s, respectively; Savage, 1999) to the gross balance, we can suppose that the anisotropic layer should be confined below the Moho.

To better locate the detected anisotropic signal at depth, it is also useful to draw a comparison with other seismological observations or with independent anisotropic datasets. In particular, Pn studies (Diaz et al., 2013) give information about anisotropy directions just beneath the Moho discontinuity and the anisotropy detected by surface waves (Zhu et al., 2015) also represent greater depth but generally with a lower definition. A comparison between our results and those from these independent methods may support (or be in opposition) with the hypothesis of a similar and continuous deformation pattern from lithospheric to asthenospheric mantle.

It is also good practice to include some additional structural information, such as the Moho depth (from the EPcrust model of Molinari and Morelli, 2011, or from the receiver function analysis of Miller and Piana Agostinetti, 2012), or the depth of the lithosphere-asthenosphere boundary (LAB, from receiver function analysis of Miller and Piana Agostinetti, 2012 and Belinić et al., 2018), or a comparison with the absolute plate motion direction as an indicator of the active asthenosphere contribution. We integrate all of the described information in each domain with the SKS anisotropy, as shown in Figure 7. In the first two maps (panels A and B), the station-averaged SKS measurements are compared with the Pn anisotropy (Diaz et al., 2013) and the surface wave azimuthal anisotropy (Zhu et al., 2015), respectively. Panel C shows the topography along the CASE profile with the seismic stations located on the boundaries of each domain. In panel D, the location of the anisotropic layer, as inferred from delay time value, calculated for 4% (cyan) and 5% (blue) of anisotropy and corrected with the Moho depth (from EPcrust model; Molinari and Morelli, 2011), is compared with the Moho (Miller and Piana Agostinetti, 2012) and LAB (Miller and Piana Agostinetti, 2012; Belinić et al., 2018) depth estimated by previous works. In panel E, the mean anisotropic direction (calculated each 20 km steps) is compared with the interpolation of the Pn and surface azimuthal anisotropy directions along the CASE profile.

In Domain 1, the SKS and Pn anisotropy directions show a very good agreement (Figure 7, panels a, b, and e), with homogeneous NW-SE direction inland and E-W direction in the Tyrrhenian sea. This trend, which is continuous in most of the domain, slightly changes close to the eastern boundary, where the Pn and SKS directions start to deviate from each other. The agreement in the direction of Pn and SKS anisotropies supports the argument that there is a vertical coherency in the deformation processes, from lithospheric to asthenospheric mantle. In Domain 1, part of the detected anisotropy is from the asthenosphere. Indeed, delay times show high values (up to 3 s), suggesting a thickness for the anisotropic layer of 180–220 km (cyan and blue volumes in Figure 7D), which is greater than the 100 km LAB depth estimated by previous works (orange crosses in Figure 7D). Our measurements, having the same direction toward the Thyrrenian sea and inland, without any back-azimuthal dependence, support the hypothesis that there is the same anisotropy direction above (toward the sea) and below (inland) the slab. This behavior has been already proposed by Baccheschi et al. (2011), who found an agreement between SKS shear wave splitting measurements made and S phases from Thyrrenian subduction deep earthquakes, and so with rays crossing the upper mantle above the slab. A coherent deformation between litho-asthenospheric domains or a mantle flowing in the shallower asthenosphere could be reasonably invoked to explain the agreement between the SKS fast axes direction with 1) the Pn direction, 2) the strike of most main fault in the area, and 3) the disagreement with the absolute plate motion of Eurasia and Africa plates in the HS2-NUVEL1A hot-spot reference frame (arrows in blue and orange, respectively, in Figures 7A,B). This last point indicates that the deformation processes are not completely driven by the asthenosphere mantle flow and this could be justified by the presence of a pressure gradient-driven mantle flow or by the presence of small scale convection of upwelling mantle (Rychert et al., 2020), we cannot exclude these hypotheses.

The five stations belonging to Domain 2 (MELA, APRC, SGRT, CAPA, and MSAG) are located just above the Apulia platform bordered in the west by the Brandanic foredeep (Br in Figure 1A) and by the Adriatic Sea to the east. Here, the Pn and SKS directions are still in nearly good agreement (Figure 7, panels a and e), even if partial rotation could be seen in correspondence of some of the stations in the Apulia platform. Both datasets show a gradual rotation from NNW-SSE to N-S and NE-SW direction, moving toward the north-east. The thickness of the anisotropic layer is in the order of 100–140 km (blue and cyan lines, Figure 7D), which when compared to the estimation of the LAB depth (80–120 km) supports the possibility of a deformation pattern continuous from the lithospheric mantle to the asthenosphere, even if not so deep as in Domain 1. If we can hypothesize a coherence in the deformation pattern with depth, we should take into account that the back-azimuthal variation in anisotropy direction (Figure 6) is a proxy to lateral changes of the deformation trend. Shear wave splitting measurements obtained by west-coming events show the typical Apennines direction, which is attributed to the sub-slab mantle deformed by Calabrian slab retreat (Baccheschi et al., 2007, 2011). Meanwhile, measurements obtained by events east-coming show a N-S to NNE-SSW direction, which is in agreement with other previous measurements along the Adriatic coast and attributed to a proper anisotropy of the Adria mantle, and is not deformed by a slab retreat process but possibly by dragging forces (Salimbeni et al., 2013; Baccheschi et al., 2007, 2008, 2011).

The stations of Domain 3 are located partially in the Italian (TREM) and Croatian (CA06A and CA06B, LSTV, CA08A, CA09A, CA05A, HVAR) islands of the Adriatic Sea and

partially in the external domain of the Dinaric (MAKA, RIC, STON, DBRK, CA04A CA02A, PDG) and Albanides (TIR) chains. These two groups of stations have different behavior in terms of Pn-SKS agreement and anisotropic layer depth. The stations located in the quasi-undeformed Adria plate (from 240 to 420 km along the CASE transect) have quite similar azimuthal anisotropy directions, representing a deformation that may be located in the first 160 km of depth (Figure 7D). The only value of surface wave anisotropy falling in the 40-km-swath box of the CASE transect, agrees with the direction of the Pn anisotropy, indicating that at least in the first 100 km of depth the anisotropy is coherent (Figure 7E). In addition, the N-S and NE-SW directions agree with the SKS-splitting results obtained by Salimbeni et al. (2013), which is interpreted as a proper Adria mantle anisotropy, perhaps related to the microplate dragging traces. However, following the obtained values of the thickness and location at depth of the anisotropic source, and considering the lack of information about the LAB depth in the area, we cannot exclude that part of the anisotropic material is at asthenospheric mantle depth.

The easternmost stations of the Domain 3, located inland (from 420 to 520 km), show instead a clear disagreement (almost 90° rotation) between Pn and SKS anisotropy directions (Figure 7E), and the thickness of the anisotropic layer is not much different from the LAB depth (Figure 7D). This data are in agreement with the presence of a complex anisotropic distribution (with fossil or layered anisotropy), with the shallower Pn (NW-SE) direction and the deeper SKS (NE-SW), as already proposed by Subašić et al. (2017), who moreover interpreted SKS directions as the asthenospheric mantle flowing through the slab gap beneath the central Dinarides. A complex anisotropic structure is also supported by the back-azimuthal dependence of measurements in this domain: teleseismic events coming from NE (shown in green in Figure 6) give a NE-SW mean direction, which is very different from those of the other sectors and is more similar to a NNW-SSE one. This discrepancy between shallow and deep anisotropy directions, which is unique all around the Adriatic coasts, induced us to research the presence of possible conditions for different types of anisotropy with respect to the A-type, which is used for the interpretation of all the study regions. However, we did not find any indicator of high stress, low temperature, or the presence of an amount of water in the mantle (Long and Becker, 2010), although there were favorable indications to the use of B-type or other anisotropy types for the interpretation.

The five stations (BBLS, BLY, CA01A, CA03A, and DIVS) in Domain 4 are in the internal part of the Dinarides chain. The prevailing SKS direction is NW-SE, parallel to the chain and to the prevailing alignment of faults, and in agreement with the Pn direction, at least in the northwestern part of this domain (Figure 7, panels a and e). Indeed, Pn anisotropy shows a general disagreement toward the easternmost part of the region (Figure 7A). These changes occur around 44°N, 19°E, where the delay time of Pn is very low. The anisotropic material is estimated as 80–180 km thick (Figure 7D). Recently, Song et al. (2019) focused on the seismic properties in the area of the Pannonian basin, Moesian Platform, and East Carpathians. They evidenced how the NW-SE direction (with an average delay time of 1.23 s) should be located at an asthenospheric depth, due to the toroidal mantle flow induced by the Adriatic subduction (in its northern portion) that influenced this and adjacent regions. The same conclusion about the depth of the anisotropy was obtained by Petrescu et al. (2020b), but with a more consistent contribution of fossil anisotropy, especially in the cratonic region of the Moesian Platform. Similarly to regions adjacent to Domain 4 and with the support of new measurements, the presence of a complex anisotropy structure is plausible, especially in the eastern part of the region, where the Pn and SKS measurements disagree, and where most of the obtained measurements are null (shown in green in Figure 6B).

Comparison with tomographic images

The Apennines and Dinarides chains are involved in complex interactions at depth, as pointed out by several tomographic images obtained with different methods. Tomographies are fundamental in the interpretation of the seismic anisotropy measurements. In Figure 8, the averaged SKS-splitting directions for new and previous measurements are superimposed on the classical Vp anomaly images of Piromallo and Morelli (2003) (A) and the newest Vs anomaly tomography by El-Sharkawy et al. (2020) (B), both at 150 km depth.

The distribution of shear wave splitting direction in the region interested by the CASE project seems to mimic the main geodynamic features highlighted by the seismic tomography maps. In particular, in the southern part of the Apennines chain the measurements rotate around the Calabrian arc (label 1 in Figure 8). This feature is interpreted by Civello and Margheriti (2004) as a toroidal flow of the sub-slab mantle, which is pushed by the retreating of the southern margin of the Apennines arc toward south-east.

On the one hand, at depths shallower than 250 km, seismic tomography maps show the presence of a slab gap in the central Apennines, particularly at its southern edge. On the other hand, the prevailing rotation of the SKS measurements is found from chain-parallel direction to E-W toward the Tyrrhenian Sea. These observations allow us to speculate that the mantle flows throughout the slab gap at shallow depths and because of the limited dimension of the slab window, it is likely that part of the deformed mantle is still aligned in the same direction found in the Northern Apennines (i.e., parallel to the belt). Moving toward the Adriatic region, fast axes are oriented mainly in a N-S and NE-SW direction, characterizing the stations of Domains 2 and 3. Although the main directions that are the same, we distinguish

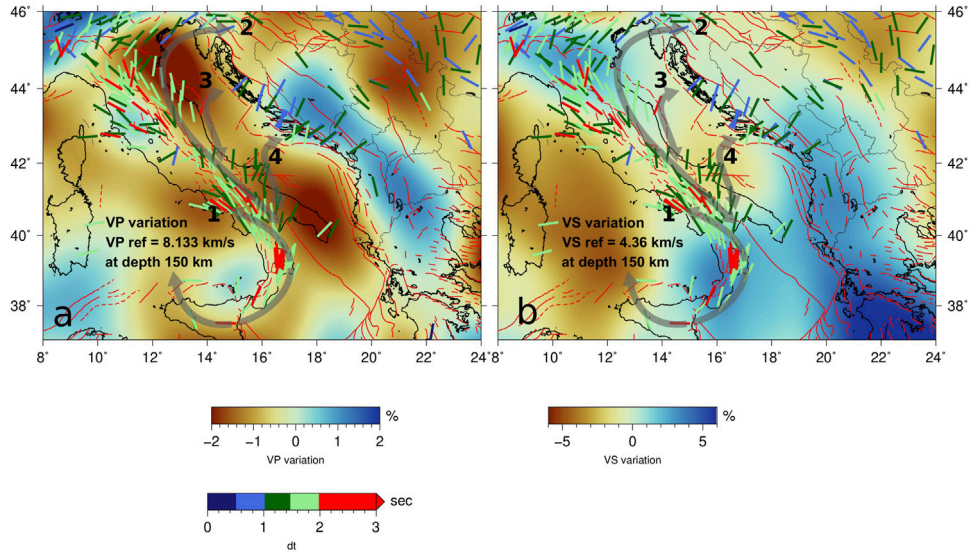

FIGURE 8
A comparison between averaged SKS measurements from this and previous works (Margheriti et al. , 2003; Civello and Margheriti, 2004; Margheriti et al., 1996; Plomerová et al., 2006; Baccheschi et al. 2007, 2008, 2011; Salimbeni et al. 2008, 2013; Subašić et al., 2017; Song et al., 2019) and the Vp **(a)** and Vs **(b)** tomography maps of Piromallo and Morelli (2003) and El-Sharkawy et al. (2020), respectively, and plotted at the 150 km depth. Each mean SKS direction is plotted as a stick parallel to the fast axes and colored with the delay time value. In both maps, the main interpretation described in the text are also sketched as toroidal flow around the sub-slab Calabrian arc (1), the mainstream flux beneath the Apennines entering in the northern (2), central (3), and southern part, and (4) of the Dinaric chain. "Roma" color map (Crameri, 2018a; 2018b) is used to plot the tomographic images.

these two domains because of differences in terms of agreement with Pn anisotropy and, especially at the border with the Dinarides, our result shows a 90° rotation. This could imply that these two domains have undergone distinct deformational processes.

The agreement of the SKS fast axes directions with the Pn anisotropy (as found for Domain 2) and an estimation of the thickness of the anisotropic layer of 100–140 km (deeper than LAB) are in agreement with a coherent deformation with depth, acting up to the asthenosphere. Moreover, the new anisotropy directions are in agreement with those previously measured by Salimbeni et al. (2013) and also with their interpretation: SKS shear wave splitting directions are aligned to the traces of the Adria microplate motion (D'Agostino et. al, 2008) in the northern Adriatic foreland. This pattern can be attributed to the Adria mantle, which is undeformed by Apenninic slab retreat and possibly related to a drag-effect of the Adria plate motion.

To interpret the shear wave splitting distribution for stations of Domain 3 taking also into account the uncertainties about slab discontinuities, we select the recent Rayleigh surface waves tomography by Belinić et al. (2021) who use data from 98 seismic stations located in the Dinaric region, which allow them to illuminate in greater detail the Adriatic and Dinarides areas. In Figure 9 this new tomography is mapped to discuss the mean SKS results for Domains 3 and 4. The shallow high velocity body that the authors interpreted as the underthrusting Adria plate beneath the Dinarides is continuous from the top to 100–150 km of depth (Figure 9A). At greater depth, a low velocity area exists and extends from the northern to the central part of Dinarides, and disappears beneath the southern Dinaric chain and Hellenides, where the slab is continuous up to depth (Figure 9B). The high velocity body dips toward NE, reaching the deepest point around 44°N, 19°E (green star in Figure 9). From the Dinarides coast toward this point, that is the internal part of the chain, we see a complete disagreement between SKS and Pn anisotropies, which is oriented almost at 90°. This framework is in agreement with lateral and vertical variations of the anisotropy, associated with the fact that the SKS-splitting measurement for stations of Domain 3 suffer from back-azimuthal dependence. The hypothesis is that at shallower depth in the lithospheric mantle, the deformation is represented by the direction of the Pn anisotropy, which is parallel to the strike of the chain and to main faults. At greater depth, the dominant direction is detected by the SKS measurements, almost parallel to the absolute plate motion of Adria in a no net-rotation reference frame (chain-perpendicular). The deepest contribution would occur completely beneath the shallower high velocity body, thus beneath the Dinarides chain, where the slab gap is wider (label 3 in Figure 9). In the region that borders the slab window (label 4 in Figure 9), the deepest mantle flow should follow the dip of the high velocity body (Figure 9C), and it is forced to have a dipping component resulting in a 3D orientation of the fast axes. This hypothesis could also justify:

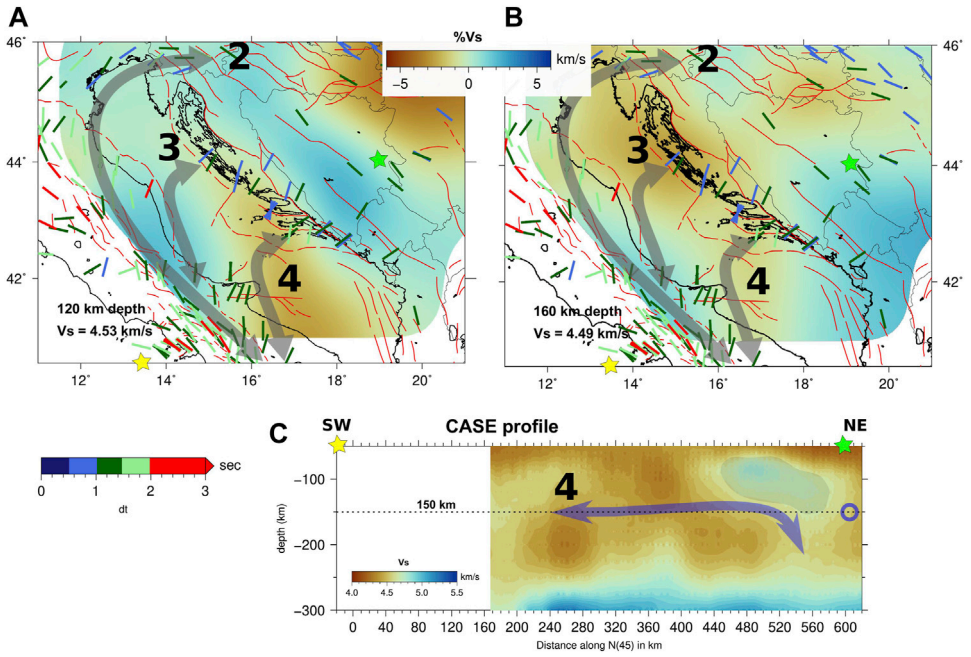

FIGURE 9
Comparison between averaged SKS measurements taken from this and previous works (Civello and Margheriti, 2003, 2004; Plomerová et al., 2006; Baccheschi et al. 2007, 2008, 2011; Salimbeni et al. 2008, 2013; Subašić et al., 2017; Song et al., 2019) and the Rayleigh surface wave tomography of Belinić et al. (2021) at 120 **(A)** and 160 **(B)** km depth. In agreement with Figure 8, we used the same "Roma" color maps (Crameri, 2018a; 2018b) and color scheme for the delay time values. In **(C)**, the tomographic section of Belinić et al. (2021) along the CASE profile is plotted and the simple interpretation of the direction of the anisotropy just before (chain-perpendicular), beneath (dipping), and after (chain-parallel) the Dinaric chain is superimposed. Stars in yellow indicate the start point of the CASE profile (as in Figure 3), while those in green indicate the deepest point of the Dinaric slab (44°N, 19°E). In both maps, the main interpretation described in the text are also sketched as toroidal flow around the sub-slab Calabrian arc (1), the mainstream flux beneath the Apennines entering in the northern (2), central (3), and the southern part (4) of the Dinaric chain.

1) The low delay times detected at the stations located along the Dinarides coast (less than 1.4 s in this work, 0.6–1 s in Subašić et al., 2017) when compared to the classical upper mantle contribution (~2 s; Savage, 1999) because the SKS phases do not cross perpendicularly the fast axes confined in a single horizontal layer.
2) The high number of null measurements found in the area, which is interpreted as due to the complexity of the anisotropic structure.

In correspondence with the deepest part of the slab, under the internal Dinarides, SKS measurements become again chain-parallel with NW-SE orientation (Domain 4). These directions agree with those found by Song et al. (2019), who interpreted them as related to an asthenospheric mantle flow generated by the toroidal flow around the northern Adria plate. In addition, Qorbani et al. (2016) found similar results, interpreting them as the consequence of the oblique compression of the Adriatic plate toward the northeast. Both of these works focus on the generation of a large-scale mantle flow around the Adria plate, flowing through the Pannonian basin and toward the south-eastern part of the internal Dinarides, where it is diverted in its southern part (Petrescu et al., 2020). This deflection generates complexity in the anisotropic structure, which is evidenced by the presence of two-layers anisotropy in the southern Carpathian (Song et al. 2019; Petrescu et al., 2020b), and by the disagreement between SKS and Pn anisotropy direction that we have detected (Figure 6). Comparing our measurements with the latest Rayleigh tomographic images (Figure 9), we cannot exclude, despite the low amount of anisotropy data, that the flow coming from the Apennines side could merge to the main one, especially where the slab gap beneath the Dinarides is wider; that is, in its central and northern part (labels 2 and 3 in Figure 9).

Comparison with geodynamic models

Recent works have attempted to reproduce the mantle flow direction with numerical and experimental simulations. In particular, Király et al. (2018b) simulated the behavior of the mantle flow in the context of the double subductions of the Adriatic plate with slab-gap generation as the origin of the Apennines chain. They demonstrated that in the case of outward double-sided subduction, the approach of the two subduction zones (Király et al. 2018a) generates an intense driving force in the sub-slabs mantle, resulting in an intense escaping flow toward the north and the south. When the slab window starts to subduct, the flow has

an additional escape way through the window, generating the classical toroidal flow that was already mentioned (flow 1 in Figure 8). In the absence of a slab window, the flow follows the edge of the slabs to find an outward way. The escaping flow that is generated will be asymmetric.

The distribution of SKS measurements presented in this work agree well with this simulation. The seismic anisotropy distribution found under the Italian peninsula is coherent with the presence of a slab window because the measurements at the stations located along the Thyrrenian coast and in the inner part of the southern Apennines, draw the toroidal flow around the remnant Calabrian slab (flow 1 in Figure 8). However, the occurrence of the slab gap also has an effect in the distribution of the mantle flow on the opposite side, in our case beneath the Dinarides. In light of the new Rayleigh tomographic images (Belinić et al., 2021), the sub-slab mantle could form the toroidal flow around the Dinaric slab only in its northern region because in its central and southern part the slab gap is not wide enough or absent (flows 2 and 3 in Figure 9 a and b, sections H-H′ and I-I′ in Figure 7 of Belinić et al. 2021). This mainstream toroidal flow should continue or end in the central/southern part of the internal Dinarides, where the SKS-splitting measurements are oriented chain-parallel (stations of Domain 4) and where previous work inferred the deformation at the asthenospheric depth (Song et al., 2019; Petrescu et al., 2020b).

Király et al.'s (2018b) model showed that after the slab break-off in the Apennines subduction zone, the slab pull force was reduced and this allowed the Adriatic plate to move more easily toward the Dinarides, as also confirmed by GPS measurements (Serpelloni et al., 2013). Following this hypothesis and considering the agreement between SKS, Pn, and absolute plate motion direction for the stations of the Domain 2 and 3, all of them oriented in the NE-SW direction, the possible litho-asthenospheric mechanism could be the drag-effect generated by the Adria plate, which could affect the structure beneath it (Salimbeni et al., 2013). Moreover, the absolute plate velocity of the Adria plate in the no-net rotation reference frame is on the order of ~3 cm/y, which is just beneath the minimum estimated by Debayle and Ricard (2013) needed for generating anisotropy at the base of the lithosphere, that is on the order of 4 cm/y. The model proposed by the authors is, however, at global scale and, as they attested in their work, locally the anisotropy could also be generated beneath a slower plate.

As a consequence of the motion of Adria plate toward the southern portion of the Dinarides (toward NE) and of the presence of the continuous slab imaged by the new seismic tomography maps, the mantle driven by the plate movement should be forced to follow the dip of the slab generating in the eastern part of the Adria plate. This non-horizontal mantle deformation could explain the low delay time values and the presence of null measurements, which are found at inland stations of Domain 3 (flow 4 in Figures 8, 9). Under this hypothesis, the NE-SW fast axis direction, perpendicular to the chain, may be related to the slab dipping direction.

Conclusion

In this work, we presented the results of the shear wave splitting analysis performed along a continuous transect from the internal part of the Apennines toward the southwestern edge of the Pannonian basin. The integration of the data from temporary and permanent seismic stations allowed us to study the seismic anisotropic properties and their variation across the entire area. In the Apennines, our new measurements confirmed the previous shear wave splitting studies, corroborating the interpretation that the asthenospheric mantle deformation (NW-SE) is due to the Calabrian slab retreat and, moving toward the Adriatic coast, the N-S to NNE-SSW directions are attributed to an undeformed Adria mantle.

In the Dinarides area, the anisotropy detected by the fast axis direction is complicated by different sources, which is more consistent with a fossil (chain-parallel) and active mantle flow (chain-perpendicular) deformation in the external part of the chain, and a more asthenospheric flow (chain-parallel) toward the internal area. The distribution of seismic anisotropy found in this paper is consistent with a mantle flow circulation around the main discontinuities present in the area (Apennines and Dinarides slab gaps), which is in agreement with the last tomography and geodynamics models proposed for the Central/Western Mediterranean area.

Data availability statement

The datasets presented in this study can be found in online repositories. The names of the repository/repositories and accession number(s) can be found in the article/ Supplementary Material.

Consortium

Zoran Božović, RHMZ RS, Republic Hydrometeorological Service of Republic of Srpska, Banja Luka, Bosnia and Herzegovina; John Clinton, ETH, Switzerland; Iva Dasović, University of Zagreb, Croatia; Ciriaco D'Ambrosio, INGV, Italy; Marijan Herak, University of Zagreb, Croatia; Dejan Jarić, RHMZ RS, Republic Hydrometeorological Service of Republic of Srpska, Banja Luka, Bosnia and Herzegovina; Edi Kissling, ETH, Switzerland; Salvatore Mazza, INGV, Italy; Irene Molinari, INGV, Italy; Snježan Prevolnik, University of Zagreb, Croatia; Simone Salimbeni, INGV, Italy; Josip Stipčević, University of Zagreb, Croatia; Vesna Šipka, RHMZ RS, Republic Hydrometeorological Service of Republicof Srpska, Banja Luka, Bosnia and Herzegovina

Author contributions

SS, SPo, and SPr contributed to the analysis of the data SS and SPo conceptualizing the results and write the first draft of the

paper. IM, JS, and ID contributed on the design and to fund the project. All authors contributed to manuscript revision, read, and approved the submitted version.

Funding

The AlpArray-CASE project and the fieldwork was supported by the AlpArray Switzerland funded by the Swiss-AlpArray SINERGIA project CRSII2_154434/1 by Swiss National Science Foundation (SNSF) and by FISR project (2017) "*Centro di studio e monitoraggio dei rischi naturali dell'Italia centrale*" funded by INGV.

Acknowledgments

All data for this study are presented in the manuscript or may be acquired through sources cited. Seismic data utilised in this work are archived at the EIDA datacenters (https://www.orfeus-eu.org/data/eida/) as: MN: Mediterranean Very Broadband Seismographic Network https://doi.org/10.13127/SD/fBBBtDtd6q: CR: Croatian Seismograph Network https://doi.org/10.7914/SN/CR: IV: Italian National Seismic Network https://doi.org/10.13127/SD/X0FXnH7QfY: SJ: Serbian Seismological Network: 8X: Central Adriatic Seismic Experiment (2016-2019): http://data.datacite.org/10.12686/alparray/8x_2016. Figures have been prepared using the Generic Mapping tools (Wessel and Smith, 1998). The manuscript benefited from constructive comments by Lara S. Wagner and two reviewers.

Conflict of interest

The authors declare that the research was conducted in the absence of any commercial or financial relationships that could be construed as a potential conflict of interest.

Publisher's note

Supplementary material

The Supplementary Material for this article can be found online at: https://www.frontiersin.org/articles/10.3389/feart.2022.881138/full#supplementary-material

SUPPLEMENTARY FIGURE S1
Example of quality of shear wave splitting results obtained from the analysis: (A) single shear wave splitting measurement that after the visual inspection we considered of "good" quality. The quality is assessed considering the isolation of the phase, the presence of the energy on the transverse component, the linearization of the particle motion after the removal of the energy, the quantity of energy reduction and the error distribution of the splitting parameters obtained. (B) null measurement obtained after the visual inspection. In this case the lack of the energy on the transverse component and the linear particle motion in its origin, help us to consider this a null measurement.

SUPPLEMENTARY FIGURE S2
Map of the single shear wave splitting measurements of "good", "average" and "poor" quality obtained in this work. In each map, the single shear wave splitting measurement is plotted as line sticks oriented parallel to the fast axes and scaled with the delay time value. In each map, yellow circles and squares are temporary and permanent stations composing the network used. Results from previous works are plotted in white (from SplitLab database; Barruol et al., 2009; Wüstefeld et al., 2009).

SUPPLEMENTARY TABLE S1
List of the shear wave splitting measurements obtained in this work

SUPPLEMENTARY TABLE S2
List of the null measurements obtained in this work

SUPPLEMENTARY TABLE S3
List of the mean shear wave splitting measurements calculated for each station

References

Auer, L., Boschi, L., Becker, T. W., Nissen-Meyer, T., and Giardini, D. (2014). Savani: A variable-resolution whole-mantle model of anisotropic shear-velocity variations based on multiple datasets. *J. Geophys. Res. Solid Earth* 119, 3006–3034. doi:10.1002/2013JB010773

Baccheschi, P., Margheriti, L., Steckler, M. S., and Boschi, E. (2011). Anisotropy patterns in the subducting lithosphere and in the mantle wedge: A case study—the southern Italy subduction system. *J. Geophys. Res.* 116, B08306. doi:10.1029/2010JB007961

Baccheschi, P., Margheriti, L., and Steckler, M. S. (2007). Seismic anisotropy reveals focused mantle flow around the Calabrian slab (Southern Italy). *Geophys. Res. Lett.* 34, L05302. doi:10.1029/2006GL028899

Baccheschi, P., Margheriti, L., and Steckler, M. S. (2008). SKS splitting in southern Italy: Anisotropy variations in a fragmented subduction zone. *Tectonophysics* 462, 49–67. doi:10.1016/j.tecto.2007.10.014

Barruol, G., Wuestefeld, A., and Bokelmann, G. (2009). *SKS-Splitting-database*. Université de Montpellier, Laboratoire Géosciences Available at: http://splitting.gm.univ-montp2.fr/DB/. doi:10.18715/sks_splitting_database

Belinić, T., Kolínský, P., and Stipčević, J. (2021). Shear-wave velocity structure beneath the Dinarides from the inversion of Rayleigh-wave dispersion. *Earth Planet. Sci. Lett.* 555, 116686. doi:10.1016/j.epsl.2020.116686

Belinić, T., Stipčević, J., Živčić, M., and AlpArrayWorking Group, the (2018). Lithospheric thickness under the Dinarides. *Earth Planet. Sci. Lett.* 484, 229–240. doi:10.1016/j.epsl.2017.12.030

Bigi, G., Cosentino, D., Parotto, M., Sartori, R., and Scandone, P. (1990). Structural model of Italy, 1:500.000, quaderni de La ricerca scientifica. *CN.R.* 114 (3).

Bijwaard, H., and Spakman, W. (2000). Non-linear global P-wave tomography by iteratedlinearized inversion. *Geophys. J. Int.* 141, 71–82. doi:10.1046/j.1365-246X.2000.00053.x

Bousquet, R., Schmid, S. M., Zeilinger, G., Oberhänsli, R., Rosenberg, C., Molli, G., et al. (2012). Tectonic framework of the Alps. *CCGM/CGMW*.

Buttles, J., and Olson, P. (1998). A laboratory model of subduction zone anisotropy. *Earth Planet. Sci. Lett.* 164, 245–262. doi:10.1016/S0012-821X(98)00211-8

Chiarabba, C., Jovane, J., and DiStefano, R. (2005). A new view of Italian seismicity using 20 years of instrumental recordings. *Tectonophysics* 395, 251–268. doi:10.1016/j.tecto.2004.09.013

Civello, S., and Margheriti, L. (2004). Toroidal mantle flow around the Calabrian slab (Italy) from SKS splitting. *Geophys. Res. Lett.* 31, L10601. doi:10.1029/2004GL019607

Crameri, F. (2018b). Geodynamic diagnostics, scientific visualisation and StagLab 3.0. *Geosci. Model. Dev.* 11, 2541–2562. doi:10.5194/gmd-11-2541-2018

Crameri, F. (2018a). Scientific colour maps. *Zenodo*. doi:10.5281/zenodo.1243862

D'Agostino, N., Avallone, A., Cheloni, D., D'Anastasio, E., Mantenuto, S., Selvaggi, G., et al. (2008). Active tectonics of the Adriatic region from GPS and earthquake slip vectors. *J. Geophys. Res.* 113, B12413. doi:10.1029/2008JB005860

Davis, J. C. (2002). *Statistics and data analysis in geology"*. 3rd ed. New York: Wiley, 656.

Debayle, E., and Ricard, Y. (2013). Seismic observations of large-scale deformation at the bottom of fast-moving plates. *Earth Planet. Sci. Lett.* 376, 165–177. doi:10.1016/j.epsl.2013.06.025

DeMets, C., Gordon, R. G., Argus, D. F., and Stein, S. (19941994). Effect of recent revisions to the geomagnetic reversal time scale on estimates of current plate motions. *Geophys. Res. Lett.* 21, 2191–2194. doi:10.1029/94GL02118

Díaz, J., Gil, A., and Gallart, J. (20132013)., 192. January, 310–325. doi:10.1093/gji/ggs016Uppermost mantle seismic velocity and anisotropy in the Euro-Mediterranean region from Pn and Sn tomography*Geophys. J. Int.*1

El-Sharkawy, A., Meier, T., Lebedev, S., Behrmann, J. H., Hamada, M., Cristiano, L., et al. (2020). The slab puzzle of the Alpine-Mediterranean Region: Insights from a new, high-resolution, shear wave velocity model of the upper mantle. *Geochem. Geophys. Geosyst.* 21, e2020GC008993. doi:10.1029/2020GC008993

Faccenna, C., Becker, T. W., Auer, L., Billi, A., Boschi, L., Brun, J. P., et al. (2014). Mantle dynamics in the mediterranean. *Rev. Geophys.* 52, 283–332. doi:10.1002/2013RG000444

Faccenna, C., and Becker, T. W. (2020). Topographic expressions of mantle dynamics in the Mediterranean. *Earth. Sci. Rev.* 209, 103327. doi:10.1016/j.earscirev.2020.103327

Faccenna, C. (2005). Constraints on mantle circulation around the deforming Calabrian slab. *Geophys. Res. Lett.* 32, L06311. doi:10.1029/2004gl021874

Faccenna, C., Piromallo, C., Crespo-Blanc, A., Jolivet, L., and Rossetti, F. (2004). Lateral slab deformation and the origin of the Western Mediterranean arcs. *Tectonics* 23, TC1012. doi:10.1029/2002TC001488

Froitzheim, N., Schmid, S. M., and Frey, M. (1996). Mesozoic paleogeography and the timing of eclogite-facies metamorphism in the Alps: A working hypothesis. *Eclogae Geol. Helvetiae* 89 (1), 81.

Funiciello, F., Moroni, M., Piromallo, C., Faccenna, C., Cenedese, A., Bui, H. A., et al. (2006). Mapping mantle flow during retreating subduction: Laboratory models ana- lyzed by feature tracking. *J. Geophys. Res.* 111, B03402. doi:10.1029/2005JB003792

Goes, S., Giardini, D., Jenny, S., Hollenstein, C., Kahle, H. G., and Geiger, A. (2004). A recent tectonic reorganization in the south-central Mediterranean. *Earth Planet. Sci. Lett.* 226, 335–345. doi:10.1016/j.epsl.2004.07.038

Gripp, A. E., and Gordon, R. G. (1990). Current plate velocities relative to the hotspots incorporating the NUVEL-1 global plate motion model. *Geophys. Res. Lett.* 17, 1109–1112. doi:10.1029/GL017i008p01109

Handy, M. R., Giese, J., Schmid, S. M., Pleuger, J., Spakman, W., Onuzi, K., et al. (2019). Coupled crust-mantle response to slab tearing, bending, and rollback along the Dinaride-Hellenide orogen. *Tectonics* 38, 2803–2828. doi:10.1029/2019TC005524

Handy, M. R., Schmid, S. M., Bousquet, R., Kissling, E., and Bernoulli, D. (2010). Reconciling plate-tectonic reconstructions of Alpine Tethys with the geological–geophysical record of spreading and subduction in the Alps. *Earth-Science Rev.* 102 (3-4), 121–158. doi:10.1016/j.earscirev.2010.06.002

Handy, M. R., Ustaszewski, K., and Kissling, E. (2015). Reconstructing the Alps-Carpathians-Dinarides as a key to understanding switches in subduction polarity, slab gaps and surface motion. *Int. J. Earth Sci.* 104, 1–26. doi:10.1007/s00531-014-1060-3

Helffrich, G. (1995). Lithospheric deformation inferred from teleseismic shear wave splitting observations in the United Kingdom. *J. Geophys. Res.* 100, 18195–18204. doi:10.1029/95jb01572

Hetényi, G., Molinari, I., Clinton, J., Bokelmann, G., Bondar, I., Crawford, W. C., et al. (2018). The AlpArray seismic network: A large-scale European experiment to image the alpine orogen. *Surv. Geophys.* 39, 1009–1033. doi:10.1007/s10712-018-9472-4

Ivan, M., Popa, M., and Ghica, D. (2008). SKS splitting observed at Romanian broadband seismic network. *Tectonophysics* 462, 89–98. doi:10.1016/j.tecto.2007.12.015

Kennett, B. L. N., Engdahl, E. R., and Buland, R. (1995). Constraints on seismic velocities in the Earth from traveltimes. *Geophys. J. Int.* 122, 108–124. doi:10.1111/j.1365-246x.1995.tb03540.x

Király, Á., Faccenna, C., and Funiciello, F. (2018b). Subduction zones interaction around the Adria microplate and the origin of the Apenninic arc. *Tectonics* 37, 3941–3953. doi:10.1029/2018TC005211

Király, Á., Holt, A. F., Funiciello, F., Faccenna, C., and Capitanio, F. A. (2018a). Modeling slab-slab interactions:Dynamics of outward dipping double-sided subduction systems. *Geochem. Geophys. Geosyst.* 19, 693–714. doi:10.1002/2017gc007199

Le Breton, E., Handy, M. R., Molli, G., and Ustaszewski, K. (2017). Post-20 Ma motion of the Adriatic plate: New constraints from surrounding Orogens and implications for crust-mantle decoupling. *Tectonics* 36, 3135–3154. doi:10.1002/2016TC004443

Li, C., van der Hilst, R. D., Engdahl, E. R., and Burdick, S. (2008). A new global model for Pwave speed variations in Earth's mantle. *Geochem. Geophys. Geosyst.* 9, Q05018. doi:10.1029/2007GC001806

Long, M. D., and Becker, T. W. (2010). Mantle dynamics and seismic anisotropy. *Earth Planet. Sci. Lett.* 297, 341–354. doi:10.1016/j.epsl.2010.06.036

Lucente, F. P., Margheriti, L., Piromallo, C., and Barruol, G. (2006). Seismic anisotropy reveals the long route of the slab through the Western-central Mediterranean mantle. *Earth Planet. Sci. Lett.* 241, 517–529. doi:10.1016/j.epsl.2005.10.041

Mainprice, D., Silver, P. G., Margheriti, L., Nostro, C., Cocco, M., and Amato, A. (1996). Interpretation of SKS-waves using samples from the subcontinental lithosphereSeismic anisotropy beneath the Northern Apennines (Italy) and its tectonic implications. *Phys. Earth Planet. InteriorsGeophys. Res. Lett.* 7823, 32572721–42802724. doi:10.1029/96gl02519

Margheriti, L., Lucente, F. P., and Pondrelli, S. (2003). *SKS*splitting measurements in the Apenninic-Tyrrhenian domain (Italy) and their relation with lithospheric subduction and mantle convection. *J. Geophys. Res.* 108 (B4), 2218. doi:10.1029/2002jb001793

Margheriti, L. (1998). SKS-Wave splitting and upper mantle structure: Results in the southern Apennines. *Ann. Geophys.* 414. doi:10.4401/ag-3806

Miller, M. S., and Piana Agostinetti, N. (2012). Insights into the evolution of the Italian lithospheric structure from S receiver function analysis. *Earth Planet. Sci. Lett.* 345-348, 49–59. doi:10.1016/j.epsl.2012.06.028

Molinari, I., Dasović, I., Stipčević, J., Šipka, V., Jarić, D., Kissling, E., et al. (2018). The AlpArray-CASE field team, the AlpArray-CASE working GroupInvestigation of the central adriatic lithosphere structure with the AlpArray-CASE seismic experiment. *Geofizika* 35, 103–128. doi:10.15233/gfz.2018.35.6

Molinari, I., and Morelli, A. (2011). EPcrust: A reference crustal model for the European plate. *Geophys. J. Int.* 185, 352–364. doi:10.1111/j.1365-246X.2011.04940.x

Molinari, I., Verbeke, J., Boschi, L., Kissling, E., and Morelli, A. (2015). Italian and Alpine three-dimensional crustal structure imaged by ambient-noise surface-wave dispersion. *Geochem. Geophys. Geosyst.* 16, 4405–4421. doi:10.1002/2015GC006176

Peccerillo, A. (2005). *Plio-quaternary volcanism in Italy*, 365. New York: Springer.

Petrescu, L., Pondrelli, S., Salimbeni, S., and Faccenda, M. (2020a2020). Mantle flow below the central and greater alpine region: Insights from SKS anisotropy analysis at AlpArray and permanent stations. *Solid earth.* 11, 1275–1290. doi:10.5194/se-11-1275-2020

Petrescu, L., Stuart, G., Houseman, G., and Bastow, I. (2020b). Upper mantle deformation signatures of craton-orogen interaction in the Carpathian-Pannonian region from SKS anisotropy analysis. *Geophys. J. Int.* 2105 (3), 2105–2118. doi:10.1093/gji/ggz573

Piromallo, C., and Morelli, A. (2003). *P* wave tomography of the mantle under the Alpine-Mediterranean area. *J. Geophys. Res.* 108, 2065. B2. doi:10.1029/2002JB001757

Plomerová, J., Margheriti, L., Park, J., Babuška, V., Pondrelli, S., Vecsey, L., et al. (2006). Seismic anisotropy beneath the northern Apennines (Italy): Mantle flow or lithosphere fabric? *Earth Planet. Sci. Lett.* 247, 157–170. doi:10.1016/j.epsl.2006.04.023

Pondrelli, S., Di Luccio, F., Scognamiglio, L., Molinari, I., Salimbeni, S., D'Alessandro, A., et al. (2020). The first very broadband mediterranean network: 30 Yr of data and seismological research. *Seismol. Res. Lett.* 91, 787–802. doi:10.1785/0220190195

Porritt, R. W., Becker, T. W., and Monsalve, G. (2014). Seismic anisotropy and slab dynamics from SKS splitting recorded in Colombia. *Geophys. Res. Lett.* 41, 8775–8783. doi:10.1002/2014GL061958

Qorbani, E., Bianchi, I., and Bokelmann, G. (20152015). Slab detachment under the Eastern Alps seen by seismic anisotropy. *Earth Planet. Sci. Lett.* 409, 96–108. doi:10.1016/j.epsl.2014.10.049

Qorbani, E., Bokelmann, G., Kovács, I., Horváth, F., and Falus, G. (2016). Deformation in the asthenospheric mantle beneath the carpathian-pannonian region. *J. Geophys. Res. Solid Earth* 121, 6644–6657. doi:10.1002/2015JB012604

Reiss, M. C., and Rümpker, G. (2017). SplitRacer: MATLAB code and GUI for semiautomated analysis and interpretation of teleseismic shear-wave splitting. *Seismol. Res. Lett.* 88 (2A), 392–409. doi:10.1785/0220160191

Rychert, C. A., Harmon, N., Constable, S., and Wang, S. (2020). The nature of the lithosphere-asthenosphere boundary. *J. Geophys. Res. Solid Earth* 125, e2018JB016463. doi:10.1029/2018JB016463

Salimbeni, S., Pondrelli, S., and Margheriti, L. (2013). Hints on the deformation penetration induced by subductions and collision processes: Seismic anisotropy beneath the Adria region (central mediterranean). *J. Geophys. Res. Solid Earth* 118, 5814–5826. doi:10.1002/2013JB010253

Salimbeni, S., Pondrelli, S., Margheriti, L., Levin, V., Park, J., Plomerová, J., et al. (2007). Abrupt change in mantle fabric across northern Apennines detected using seismic anisotropy. *Geophys. Res. Lett.* 34, L07308. doi:10.1029/2007GL029302

Salimbeni, S., Pondrelli, S., Margheriti, L., Park, J., and Levin, V. (2008). SKS splitting measurements beneath northern Apennines region: A case of oblique trench-retreat. *Tectonophysics* 462, 68–82. doi:10.1016/j.tecto.2007.11.075

Savage, M. (1999). Seismic anisotropy and mantle deformation: What have we learned from shear wave splitting? *Rev. Geophys.* 37, 65–106. doi:10.1029/98RG02075

Savastano, L., and Piana Agostinetti, N. (2018). Deep structure of the Southern Apennines as imaged by active and passive seismic data along the CROP-04 (crustal) reflection seismic profile. *J. Geol. Soc.* 176 (6), 1284–1290. doi:10.1144/jgs2018-201

Schlaphorst, D., Kendall, J. M., Baptie, B., Latchman, J. L., and Tait, S. (2017). Gaps, tears and seismic anisotropy around the subducting slabs of the Antilles. *Tectonophysics* 698, 65–78. doi:10.1016/j.tecto.2017.01.002

Schmid, S. M., Bernoulli, D., Fügenschuh, B., Matenco, L., Schefer, S., Schuster, R., et al. (2008). The alpine-carpathian-dinaridic orogenic system: Correlation and evolution of tectonic units. *Swiss J. Geosci.* 101 (1), 139–183. doi:10.1007/s00015-008-1247-3

Schmid, S. M., Fügenschuh, B., Kissling, E., and Schuster, R. (2004). Tectonic Map andoverall architecture of the Alpine orogen. *Eclogae Geol. Helv.* 97 (1), 93–117. doi:10.1007/s00015-004-1113-x

Selvaggi, G., and Amato, A. (1992). Subcrustal earthquakes in the northern Apennines (Italy): Evidence for a still active subduction? *Geophys. Res. Lett.* 19, 2127–2130. doi:10.1029/92GL02503

Serpelloni, E., Anzidei, M., Baldi, P., Casula, G., and Galvani, A. (2005). Crustal velocity and strain-rate fields in Italy and surrounding regions: New results from the analysis of permanent and non-permanent GPS networks. *Geophys. J. Int.* 161, 861–880. doi:10.1111/j.1365-246X.2005.02618.x

Serpelloni, E., Faccenna, C., Spada, G., Dong, D., and Williams, S. D. P. (2013). Vertical GPS ground motion rates in the Euro-Mediterranean region: New evidence of velocity gradients at different spatial scales along the Nubia-Eurasia plate boundary. *J. Geophys. Res. Solid Earth* 118, 6003–6024. doi:10.1002/2013JB010102

Silver, P., and Chan, W. (1988). Implications for continental structure and evolution from seismic anisotropy. *Nature* 335, 34–39. doi:10.1038/335034a0

Silver, P. G., and Chan, W. W. (1991). Shear wave splitting and subcontinental mantle deformation. *J. Geophys. Res.* 96 (16429–16), 16429. doi:10.1029/91jb00899

Silver, P. G., and Savage, M. K. (1994). The interpretation of shear-wave splitting parameters in the presence of two anisotropic layers. *Geophys. J. Int.* 119 (3), 949–963. doi:10.1111/j.1365-246X.1994.tb04027.x

Song, W., Yu, Y., Shen, C., Lu, F., and Kong, F. (2019). Asthenospheric flow beneath the Carpathian-Pannonian region: Constraints from shear wave splitting analysis. *Earth Planet. Sci. Lett.* 520, 231–240. doi:10.1016/j.epsl.2019.05.045

Stipčević, J., Herak, M., Molinari, I., Dasović, I., Tkalčić, H., Gosar, A., et al. (2020). Crustal thickness beneath the Dinarides and surrounding areas from receiver functions. *Tectonics* 37. doi:10.1029/2019TC005872

Stipčević, J., Tkalčić, H., Herak, M., Markušić, S., and Herak, D. (2011). Crustal and uppermost mantle structure beneath the External Dinarides, Croatia, determined from teleseismic receiver functions. *Geophys. J. Int.* 185, 1103–1119. doi:10.1111/j.1365-246X.2011.05004.x

Subašić, S., Prevolnik, S., Herak, D., and Herak, M. (2017). Observations of SKS splitting beneath the central and southern external Dinarides in the adria-eurasia convergence zone. *Tectonophysics* 705, 93–100. doi:10.1016/j.tecto.2017.03.027

van der Meer, D. G., van Hinsbergen, D. J., and Spakman, W. (2018). Atlas of the underworld: Slab remnants in the mantle, their sinking history, and a new outlook on lower mantle viscosity. *Tectonophysics* 723, 309–448. doi:10.1016/j.tecto.2017.10.004

Wessel, P., and Smith, W. H. F. (1998). New, improved version of generic mapping tools released. *Eos Trans. AGU.* 79, 579. doi:10.1029/98EO00426

Wüstefeld, A., Bokelmann, G. H. R., Barruol, G., and Montagner, J.-P. (2009). Identifying global seismic anisotropy patterns by correlating shear-wave splitting and surface-wave data. *Phys. Earth Planet. Interiors* 176 (3-4), 198–212. doi:10.1016/j.pepi.2009.05.006

Zhu, H., Bozdağ, E., Peter, D., and Tromp, J. (2012). Structure of the European upper mantle revealed by adjoint tomography. *Nat. Geosci.* 5 (7), 493–498. doi:10.1038/ngeo1501

Zhu, H., Bozdağ, E., and Tromp, J. (20152015). Seismic structure of the European upper mantle based on adjoint tomography. *Geophys. J. Int.* 201 (Issue 1), 18–52. doi:10.1093/gji/ggu492